⌘ *Author's Choice*

THE JOURNAL OF BIOLOGICAL CHEMISTRY VOL. 285, NO. 21, pp. 16330–16340, May 21, 2010

Crystal Structures of Human Choline Kinase Isoforms in Complex with Hemicholinium-3

SINGLE AMINO ACID NEAR THE ACTIVE SITE INFLUENCES INHIBITOR SENSITIVITY[*][S]

Received for publication, June 29, 2009, and in revised form, February 28, 2010 Published, JBC Papers in Press, March 18, 2010, DOI 10.1074/jbc.M109.039024

Bum Soo Hong[‡1], Abdellah Allali-Hassani[‡1], Wolfram Tempel[‡], Patrick J. Finerty, Jr.[‡], Farrell MacKenzie[‡], Svetoslav Dimov[‡], Masoud Vedadi[‡2], and Hee-Won Park[‡§3]

From the [‡]Structural Genomics Consortium and [§]Department of Pharmacology, University of Toronto, Toronto, Ontario M5G 1L7, Canada

Human choline kinase (ChoK) catalyzes the first reaction in phosphatidylcholine biosynthesis and exists as ChoKα (α1 and α2) and ChoKβ isoforms. Recent studies suggest that ChoK is implicated in tumorigenesis and emerging as an attractive target for anticancer chemotherapy. To extend our understanding of the molecular mechanism of ChoK inhibition, we have determined the high resolution x-ray structures of the ChoKα1 and ChoKβ isoforms in complex with hemicholinium-3 (HC-3), a known inhibitor of ChoK. In both structures, HC-3 bound at the conserved hydrophobic groove on the C-terminal lobe. One of the HC-3 oxazinium rings complexed with ChoKα1 occupied the choline-binding pocket, providing a structural explanation for its inhibitory action. Interestingly, the HC-3 molecule co-crystallized with ChoKβ was phosphorylated in the choline binding site. This phosphorylation, albeit occurring at a very slow rate, was confirmed experimentally by mass spectroscopy and radioactive assays. Detailed kinetic studies revealed that HC-3 is a much more potent inhibitor for ChoKα isoforms (α1 and α2) compared with ChoKβ. Mutational studies based on the structures of both inhibitor-bound ChoK complexes demonstrated that Leu-401 of ChoKα2 (equivalent to Leu-419 of ChoKα1), or the corresponding residue Phe-352 of ChoKβ, which is one of the hydrophobic residues neighboring the active site, influences the plasticity of the HC-3-binding groove, thereby playing a key role in HC-3 sensitivity and phosphorylation.

The enzyme choline kinase (ChoK,[4] EC 2.7.1.32) catalyzes the Mg·ATP-dependent phosphorylation of choline as the first step in the Kennedy (CDP-choline) pathway, in which choline is incorporated into phosphatidylcholine (1–3). In this reaction, choline is first converted into phosphocholine (Pho-Cho), which then reacts with CTP to form CDP-choline. The Pho-Cho moiety is then transferred to diacylglycerol to produce phosphatidylcholine. This pathway is a major source of phosphatidylcholine, which is a highly abundant class of phospholipids in mammalian cellular membranes and serum (2, 4). Mammalian ChoK exists as three isoforms, encoded by two separate genes (5, 6). In humans, ChoKα1 (457 amino acids) and ChoKα2 (439 amino acids) are derived from a single gene (*chk-*α) by alternative splicing, while ChoKβ (395 amino acids) is the product of a distinct gene (*chk-*β). The amino acid sequence identity is ~56% between ChoKα and ChoKβ (Fig. 1), and both *chk-*α and *chk-*β mRNAs, as well as their encoded protein isoforms, are ubiquitously expressed in diverse tissues (7). Each isoform is present as either dimers (homo- or hetero-) or as tetramers in solution and is not active in monomeric form (3), suggesting that, for higher eukaryotes, dimeric ChoK is the minimum functional form. Recently, the crystal structures of ChoK proteins from *Caenorhabditis elegans* and human have been determined, in which two monomers were dimerized in each asymmetric unit (8, 9).

ChoK is implicated in tumorigenesis, and its overexpression and elevated activity have been observed in human tumor-derived cell lines and in various primary tumors (10–14). ChoK potentiates *ras*/*rho*-induced carcinogenesis, where *in vitro* studies have shown that ChoK is constitutively active in cells transformed by ras/rho oncogenes. This results in an increased level of Pho-Cho (15–18), which is a putative novel second messenger involved in cellular proliferation (19). Likewise, inhibition of ChoK is an efficient antitumor strategy in oncogene-transformed cells and *in vivo* assays in nude mice (20, 21). Recent studies further indicate that ChoKα is extensively involved in malignancy, suggesting not only its usefulness as a

* This work was supported by the Structural Genomics Consortium, a registered charity (number 1097737) that receives funds from the Canadian Institutes for Health Research, the Canadian Foundation for Innovation, Genome Canada through the Ontario Genomics Institute, GlaxoSmithKline, Karolinska Institutet, the Knut and Alice Wallenberg Foundation, the Ontario Innovation Trust, the Ontario Ministry for Research and Innovation, Merck & Co., Inc., the Novartis Research Foundation, the Swedish Agency for Innovation Systems, the Swedish Foundation for Strategic Research, and the Wellcome Trust. Use of the Advanced Photon Source was supported by the U. S. Dept. of Energy, Office of Science, Office of Basic Energy Sciences, under Contract DE-AC02-06CH11357.

⌘ *Author's Choice*—Final version full access.

[S] The on-line version of this article (available at http://www.jbc.org) contains supplemental Figs. S1–S7, Tables S1–S3, references, and Materials I and II.

[1] Both authors contributed equally to this work.

[2] To whom correspondence may be addressed: Structural Genomics Consortium, University of Toronto, MaRS South Tower, 101 College St., Toronto, Ontario M5G 1L7, Canada. Tel.: 416-946-0897; Fax: 416-946-0588; E-mail: mvedadi@uhnres.utoronto.ca.

[3] To whom correspondence may be addressed: Structural Genomics Consortium, University of Toronto, MaRS South Tower, 101 College St., Toronto, Ontario M5G 1L7, Canada. Tel.: 416-946-3867; Fax: 416-946-0588; E-mail: heewon.park@utoronto.ca.

[4] The abbreviations used are: ChoK, choline kinase (specific isoforms are numbered); HC-3, hemicholinium-3; HPLC, high-performance liquid chromatography; WT, wild type; ITC, isothermal titration calorimetry.

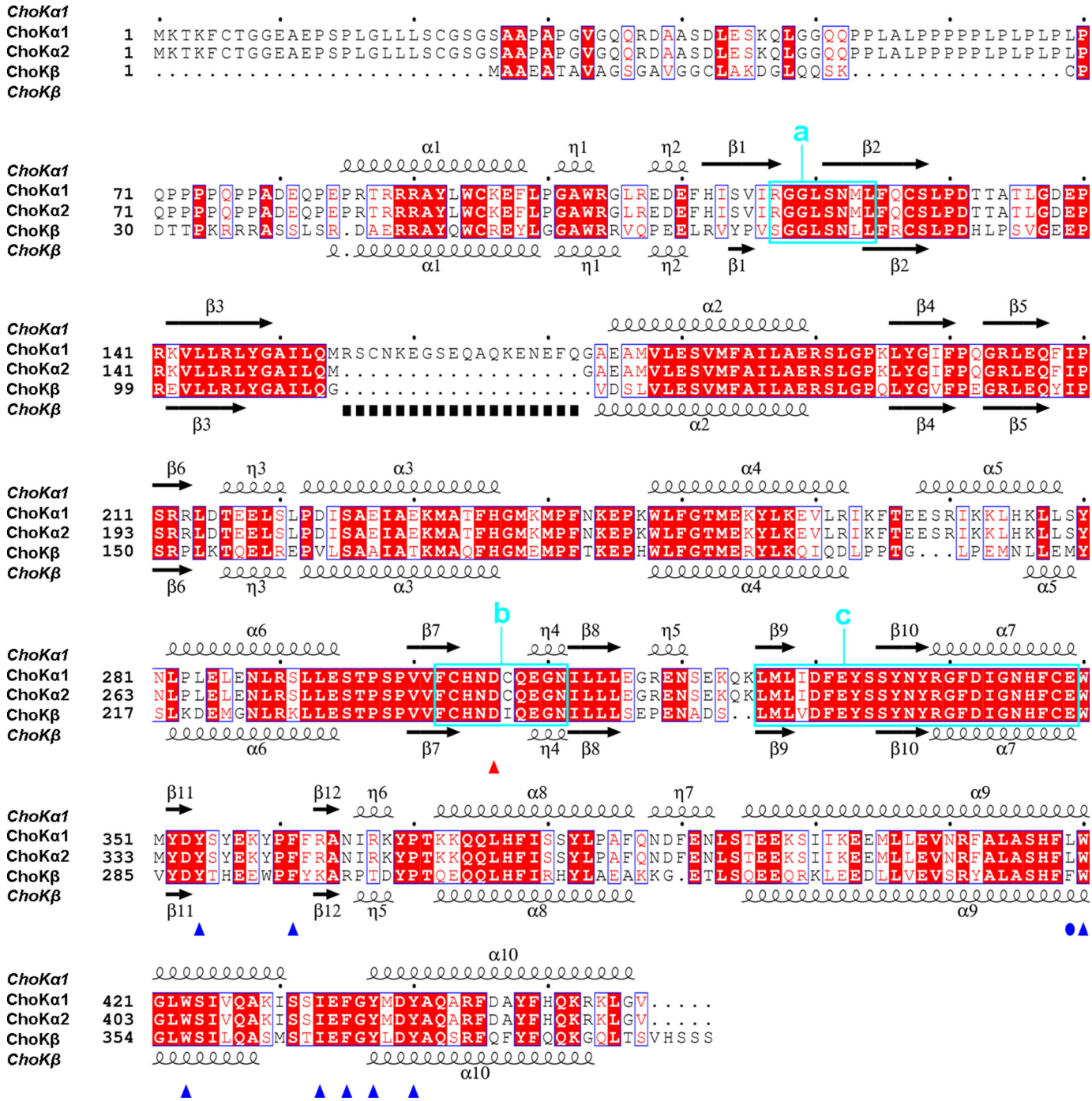

FIGURE 1. **Structure-based sequence alignment of human ChoK isoforms.** The secondary structure elements of ChoKα1 (NCBI accession number NP_001268, PDB code 3G15) and ChoKβ (NCBI accession number NP_005189, PDB code 3FEG) are placed on the *top* and the *bottom* of the alignment, respectively. Conserved residues are depicted in *white* on a *red background*. Physicochemically conserved residues are depicted in *red*. Overall conserved regions are *framed* in *blue*. In ChoKα2 (NCBI accession number NP_997634), the coding sequences that are missed due to alternative splicing are indicated by *black squares* at the *bottom*. The *blue triangles* indicate the hydrophobic residues forming van der Waals interactions with HC-3. The *blue circle* indicates the residue (Leu-419 of ChoKα1 and Phe-352 of ChoKβ) affecting the flexibility of the conserved tryptophan residue (Trp-420 of ChoKα1 and Trp-353 of ChoKβ). The *red triangle* indicates the catalytic base (Asp-306 of ChoKα1 and Asp-242 of ChoKβ) for ATP hydrolysis. The catalytically important regions suggested by Malito *et al.* (9) are *boxed* and labeled in *cyan* (*a*, ATP-binding loop; *b*, Brenner's motif; *c*, choline kinase motif). The alignment was generated with ClustalW (43) and was printed using the ESPript 2.1 software package (44).

prognostic indicator for human cancers, but also ChoKα-targeted treatment with chemical inhibitors as a novel therapeutic strategy (22–24). However, the precise mechanism of regulation of ChoK in tumorigenesis remains unclear.

In an effort to develop new anti-cancer therapies, numerous compounds have been synthesized and tested as ChoK inhibitors (20, 25–27). Most of these compounds are derivatives of hemicholinium-3 (HC-3), a known competitive inhibitor of ChoK with a structural homology to choline (Fig. 2, *A* and *B*) (28). Although several HC-3-derived inhibitors are under investigation for their potential clinical applicability, their efficacy is still uncertain. Most reported ChoK inhibitors, includ-

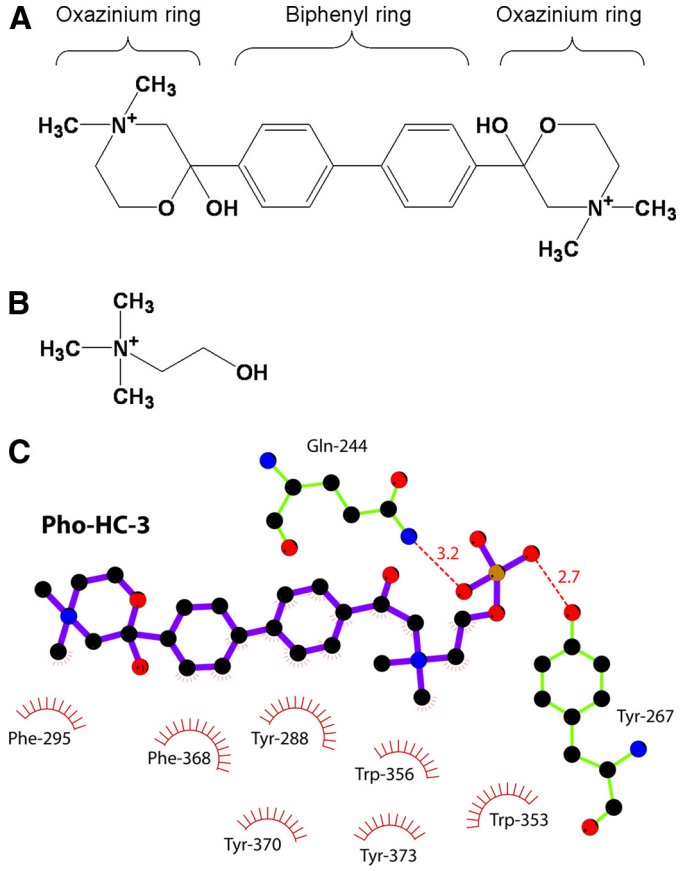

FIGURE 2. **Chemical structures of HC-3 (*A*) and choline (*B*).** Specific moieties of HC-3 are indicated at the *top* of the molecule. *C*, schematic illustration of ΔN-ChoKβ interactions with Pho-HC-3. Pho-HC-3 is represented in *ball-and-stick* and is colored *purple*. Residues forming van der Waals' interactions are indicated by an *arc* with radiating spokes toward the ligand atom they contact; those residues participating in hydrogen bonding are colored in *lime green* and shown in *ball-and-stick* representation. Hydrogen bonds are indicated as *red dotted lines* with distances in angstroms. Carbon atoms are colored in *black*, oxygen atoms are in *red*, nitrogen atoms are in *blue*, and phosphorus is colored in *orange*. The figure was generated with the program LIGPLOT (47) followed by manual editing.

ing HC-3, contain long or bulky hydrophobic aromatic chains, whereas the choline-binding pocket has an overall negative electrostatic potential (8, 9). This reinforces interest in the interaction between ChoK and potential inhibitors, but no detailed structural information has been available so far.

Here, we present the crystal structures of human ChoKα1 and ChoKβ in complex with HC-3 in the presence of adenine nucleotides. In the course of structure determination, we serendipitously discovered that the HC-3 molecule captured in the ChoKβ crystal was phosphorylated, an observation that was further confirmed by *in vitro* experiments, which showed that ChoKβ enzymatically phosphorylates HC-3. Additional experiments showed that HC-3 is a more potent inhibitor of ChoKα (α1 and α2) compared with ChoKβ. A series of substitution mutants was used to show that the unique enzymatic phenotypes of the ChoK isoforms toward HC-3 are significantly regulated by the differential flexibility of the binding groove that accommodates the inhibitor. Together, our data provide the first crystallographic model of inhibitor-bound ChoK and describe a potential mechanism of HC-3 inhibitory action at the atomic level.

EXPERIMENTAL PROCEDURES

Protein Expression and Purification—The genes encoding the N-terminally truncated ChoKα1 (residues 75–457, named herein as ΔN-ChoKα1) and ChoKβ (residues 35–395, named herein as ΔN-ChoKβ) were initially cloned downstream of the six-histidine tag of the pET28a expression vector (Novagene), and the resulting plasmids were transformed into *Escherichia coli* BL21(DE3) cells (Stratagene) by heat shock. Transformants were grown at 37 °C in terrific broth medium containing 50 μg/ml kanamycin. Once the absorbance of the culture reached ~0.7 at 600 nm, isopropyl β-D-thiogalactopyranoside (Sigma) was added to a final concentration of 0.5 mM, and the mixture was incubated overnight at 18 °C. Cells were harvested by centrifugation and suspended in a solution containing 10 mM Tris-HCl (pH 7.5), 0.5 M NaCl, 5 mM imidazole, 5% glycerol, and 1 mM Tris(2-carboxyethly)phosphine hydrochloride with protease inhibitor mixture (Sigma). Cells were disrupted by sonication, and the lysate was clarified by centrifugation. The supernatant was loaded onto a 5-ml HisTrap HP column (Amersham Biosciences) using standard fast protein liquid chromatography procedures (Amersham Biosciences), and the ChoK proteins were eluted with a 10–300 mM imidazole gradient. The peak protein-containing fractions were analyzed by SDS-PAGE, pooled, and further purified on a Superdex 200 HR column (Amersham Biosciences) equilibrated with 10 mM Tris-HCl (pH 8.0), 0.5 M NaCl, 5 mM $MgCl_2$, and 10 mM dithiothreitol. For crystallization, purified ΔN-ChoKα1 and ΔN-ChoKβ proteins were concentrated to 30 and 35 mg/ml, respectively, and stored at −80 °C.

Crystallization—Ternary complexes of ΔN-ChoK proteins with HC-3 and ADP were crystallized using the sitting-drop, vapor diffusion method at 18 °C. ADP (Sigma-Aldrich) was prepared in the buffer solution for gel filtration at a concentration of 0.5 M, while HC-3 (Sigma-Aldrich) was prepared in 100% DMSO at a concentration of 0.2 M, and both samples were kept at −20 °C until use. To achieve full occupancy of bound substrate or inhibitor, the proteins were mixed with 5- to 10-fold molar excess of ADP and HC-3 and incubated overnight at room temperature. Equal volumes of protein solution and reservoir solution were combined for crystallization. Crystals of ΔN-ChoKα1·ADP·HC-3 were grown against a reservoir buffer containing 0.1 M HEPES (pH 7.5), 25% polyethylene glycol-3350, and 0.2 M lithium sulfate. Thin, plate-like crystals appeared within 3–4 days and achieved their full size in approximately 1 week. Crystals of ΔN-ChoKβ·ADP·Pho-HC-3 were grown in 0.1 M sodium cacodylate (pH 6.5), 30% polyethylene glycol-4000, and 0.2 M ammonium sulfate. Cubic crystals appeared in 3 days and achieved their full size within a week. All of the crystals used in this study were cryoprotected in a 50:50 mixture of Paratone-N and mineral oil, and flash-frozen in liquid nitrogen.

Data Collection and Structure Determination—Data collection was carried out at the Advanced Photon Source beamline 23ID-B, and all of the diffraction data were processed using the HKL2000 package (29). Crystal structures of ΔN-ChoK proteins in complex with ADP and HC-3 were solved by the molecular replacement method using PHASER

(30) with search models based on the coordinates of human choline kinase α (PDB code 2I7Q) and β (PDB code 2IG7), respectively. The models underwent several rounds of model building, refinement, and validation with COOT (31), REFMAC5 (32), and MOLPROBITY (33), respectively. Individual isotropic temperature factors were refined with the exception of PDB code 3FEG, where individual anisotropic displacement parameters were refined. Data collection and refinement statistics are given in Table 1 and supplemental Table S2.

Preparation of Wild-type and Mutant ChoK—The wild-type full-length *chk* genes (*chk-α1*, *chk-α2*, and *chk-β*) were cloned into pET28a, and the resulting clones were used as templates to generate ChoK mutants. Four missense point mutants of ChoK isoforms were constructed using the QuikChange site-directed mutagenesis method (Stratagene) using complementary 30- to 40-nucleotide primers containing the desired mutations. All cloned constructs were verified by DNA sequence analysis prior to protein expression, and each mutant protein was purified as described above. All purified samples were concentrated to 10 mg/ml and stored at −80 °C.

Enzymatic Assay and Inhibition Study—ChoK assays were performed using either an HPLC-based method (45) or the LDH-PK-coupled assay (9). In the HPLC method, production of ADP (generated from ATP hydrolysis by ChoK) was monitored by separation and quantification of AMP, ADP, and ATP as described previously (45). Enzymatic activity of the three wild-type ChoKs (α1, α2, and β) and their mutants were determined in the presence of 1 mM ATP and different choline concentrations. Reactions were terminated by addition of two volumes of 8 M urea (5.3 M final concentration). Mixtures were filtered through a 5-kDa MWCO Amicon Ultrafree-MC filter (Millipore, Bedford, MA) prior to loading onto the HPLC column.

To determine the enzymatic activity of ChoK using HC-3 as a substrate in the presence of ADP, adenylate kinase was used to prepare [β-^{32}P]ADP from [γ-^{32}P]ATP. The mixture of hot and cold ADP was separated from ATP and AMP, and then further purified using the HPLC method as described above. The rate of radioactivity incorporation into HC-3 upon phosphorylation using either [γ-^{32}P]ATP or [β-^{32}P]ADP was determined by integration of the resolved peak using the software from the HPLC unit that was equipped with a radioactivity detector (IN/US Systems B-RAM model 4B, Primer Biotech, Ontario, Canada). Mass spectrometry was also used to detect the change in the mass of HC-3 upon phosphorylation by ChoK enzymes. A shift in the absorbance maximum of HC-3 from λ_{max} = 258.4 nm to λ_{max} = 293.9 nm upon phosphorylation was observed and used to monitor the changes as well. For complete kinetics of wild-type ChoK enzymes and their mutants as well as determining HC-3 inhibition constants (K_i values), the lactate dehydrogenase-pyruvate kinase assay was used as described previously (9) and was adapted to a 384-well plate format using a BioTek Senergy2 microplate reader, which allowed a quick and parallel determination of kinetic parameters. Kinetic values were determined using saturating concentrations of ATP. When a wide range of choline concentrations was used to determine Michaelis-Menten kinetic parameters, a nonsaturating kinetic was observed. This may be due to some degree of negative cooperativity as was previously described for yeast ChoK by Brostrom *et al.* (46). To be able to compare the kinetic parameters and the inhibition effect of HC-3, we selected a reasonable range of substrate concentrations and fitted the data to the Michaelis-Menten equation. All kinetic values reported herein are obtained in the same manner and are considered apparent values. All the measurements were done in triplicate.

Isothermal Titration Calorimetry—The ITC measurements were performed in duplicate at 25 °C using a VP-ITC microcalorimeter (MicroCal Inc.). Experiments were performed by injecting 10 μl of HC-3 (0.25- 1 mM) into a sample cell containing 20 μM ChoK protein, which was previously dialyzed extensively in degassed ITC buffer (25 mM Tris-HCl (pH 7.5), 0.2 M NaCl, and 2 mM β-mercaptoethanol). A total of 25 injections was performed with a spacing of 180 s and a reference power of 13 μcal/s. HC-3 was first dissolved at 0.2 M in 100% DMSO and was diluted in ITC buffer. Heat of dilution generated from the injected compound was subtracted from the experimental curves, and binding isotherms were plotted and analyzed using Origin (MicroCal Inc.). The data were fit to a one-site binding model equation.

RESULTS

Structural Overview of ΔN-ChoK Ternary Complexes—Crystals of HC-3-bound ΔN-ChoKα1 and ΔN-ChoKβ were obtained in the presence of ADP. Both ADP and HC-3 molecules in the ΔN-ChoKα1 crystal were well defined in initial model-phased difference Fourier maps, but the HC-3 in the ΔN-ChoKβ crystal was present in a phosphorylated form (henceforth referred to as Pho-HC-3 in the text and figures) (Fig. 3*A* and supplemental Fig. S1). Although the two ΔN-ChoK isoforms existed as dimers in solution, ΔN-ChoKβ, unlike that of ΔN-ChoKα1 (*i.e.* two monomers in the asymmetric unit), was crystallized with a monomer in the asymmetric unit of the cells, in which dimer interface was formed by interaction across crystallographic rotational axis (see supplemental Material I for details). The final models of the ternary complexes of ΔN-ChoKα1 and ΔN-ChoKβ were refined at 1.7 and 1.3 Å, respectively (Table 1 and supplemental Table S2). Both the ChoK structures exhibit the same bilobal architecture as seen in other typical kinase family proteins (34, 35). The root mean square deviation of the Cα atoms between the two ChoK ternary complex structures was 0.9 Å, whereas the individual lobes overlaid with slightly smaller deviations of 0.72 Å and 0.75 Å for the N- and C-terminal lobes, respectively. The major differences between the two ChoK structures were located at the C-terminal lobe and will be discussed in detail below. The quality of the electron density map for the two models was well defined except for several small portions. In the ΔN-ChoKα1 ternary complex, for instance, the region flanking the segment (residues 155–172), which is missing in ChoKα2 due to alternative splicing (Fig. 1), was invisible in our maps. This region was also disordered in ChoKα crystal structures previously studied (9). Likewise, residues 75–79 and 108–110 of the ΔN-ChoKβ ternary complex were not refined because of weak electron density.

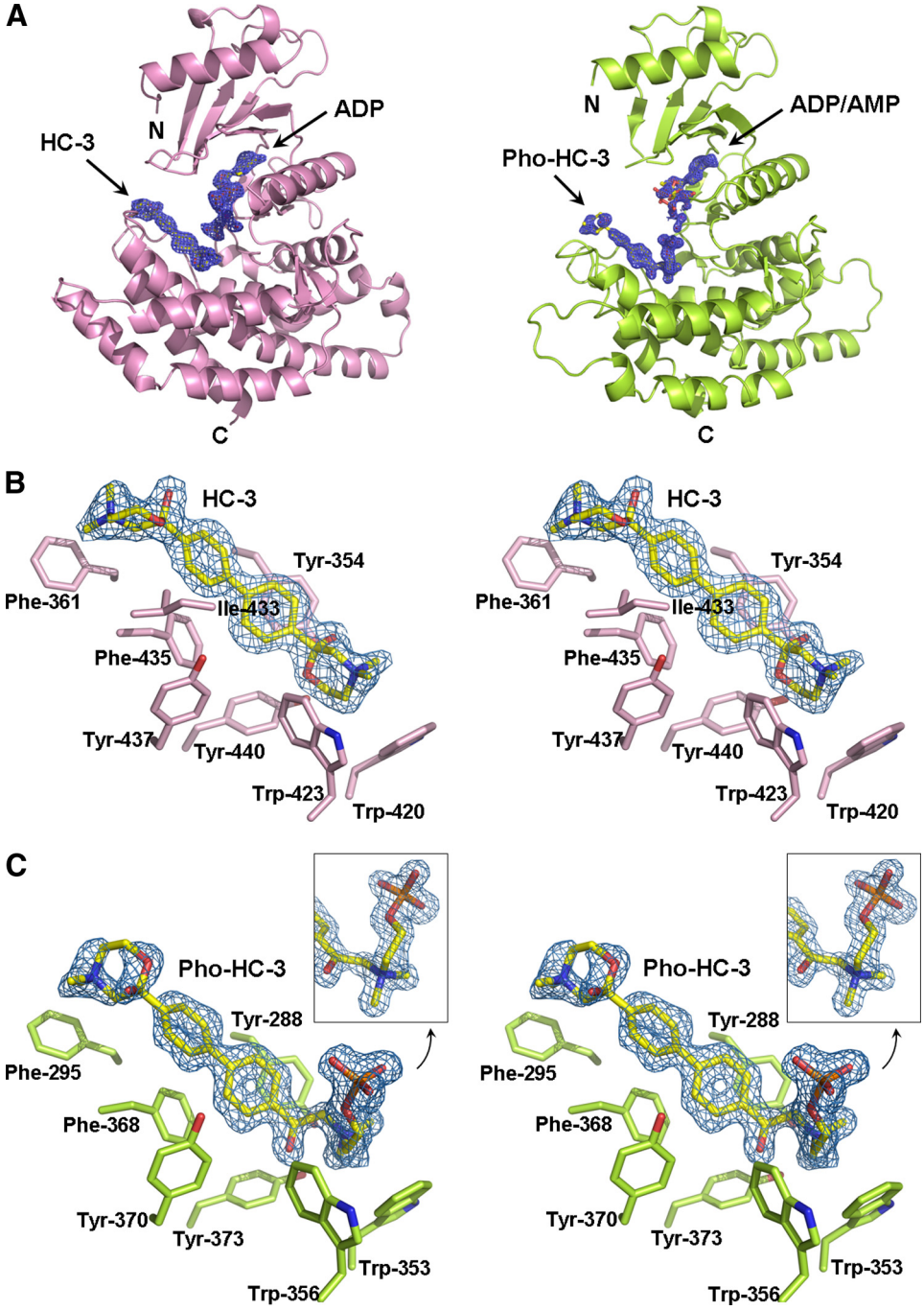

FIGURE 3. **Overall structures of ΔN-ChoK ternary complexes.** *A*, *ribbon diagrams* of the crystal structures of ΔN-ChoKα1 (*pink*) and β (*lime green*) ternary complexes. Adenine nucleotides, HC-3, and Pho-HC-3 are shown within the sigma-weighted $F_o - F_c$ omit map (*blue*) contoured at the 2.5 σ level and indicated by *arrows*. One monomer in the dimeric ΔN-ChoK models is indicated. *B*, close-up *stereo view* of the HC-3-binding site in the ΔN-ChoKα1·ADP·HC-3 complex structure. The difference Fourier map for HC-3 is drawn at a contour level of 2.5 σ. The HC-3 (*yellow*) and its surrounding hydrophobic residues (*pink*) are marked and represented in *stick mode*. *C*, close-up *stereo view* of the HC-3-binding site in the ΔN-ChoKβ·ADP·Pho-HC-3 complex structure. The difference Fourier map corresponding to Pho-HC-3 is drawn at a contour level of 2.5 σ. The Pho-HC-3 (*yellow*) and its surrounding hydrophobic residues (*lime green*) are marked and shown in *stick mode*. The *inset* displays the phosphorylated region of Pho-HC-3 at a slightly different angle. All of the figures were generated using PyMOL (DeLano, W. L. (2002) *The PyMOL Molecular Graphics System*, DeLano Scientific LLC, San Carlos, CA).

HC-3 Interaction with ΔN-ChoKα1—The crystal structure of the ΔN-ChoKα1·ADP·HC-3 complex reveals that HC-3 bound to a groove on the C-terminal lobe near the interlobe cleft in a manner where one oxazinium ring occupied the choline-binding pocket, and the other oxazinium ring was partially exposed to solvent (Fig. 3*A*). The HC-3-binding groove was lined by hydrophobic residues (Tyr-354, Phe-361, Trp-420, Trp-423, Ile-433, Phe-435, Tyr-437, and Tyr-440), and only one side of the planar HC-3 molecule contributed to the hydrophobic interaction with the groove (Fig. 3*B*). The HC-3 oxazinium ring that occupied the choline-binding pocket could be superimposed onto the choline moiety modeled from the crystal structure of ChoKα in complex with Pho-Cho (PDB code 2CKQ) (Fig. 4), providing direct structural evidence supporting the idea that HC-3 competes with choline for the same binding pocket on ChoK (28).

The ΔN-ChoKα1 model showed that ADP and two magnesium ions were located at the nucleotide-binding site of the N-terminal lobe (supplemental Fig. S1*A*). In addition, the extra tetrahedral electron density was observed close to the β-phosphate of ADP and was assigned as a sulfate ion originating from the crystallization buffer (supplemental Fig. S1*A*). ADP interacted either directly or indirectly with multiple residues (*i.e.* Arg-117, Arg-146, Asp-306, Asn-311, Asp-330, and Glu-332) and water molecules, and its phosphate oxygens coordinated two magnesium ions (see supplemental Material II for details and supplemental Fig. S2*A*). The ΔN-ChoKα1 structure further suggested potential structural roles of some residues near a nucleotide-binding site that have not been previously defined. Arg-117 forming a portion of an ATP-binding loop (residues 117–124) pointed toward the β-phosphate of bound ADP, thereby positioning the nucleotide for enzymatic catalysis (supplemental Fig. S1*A*). Glu-332, which belongs to the highly conserved ChoK motif of the C-terminal lobe (9), participated directly in coordination of the second magnesium ion (supplemental Fig. S2*A*).

HC-3 Phosphorylation by ΔN-ChoKβ—In the crystal structure of the ΔN-ChoKβ ternary complex, HC-3 was bound in the same way as described for the ΔN-ChoKα1 model (Fig. 3*C*), which, with one exception (Ile-366), was also reflected in the

TABLE 1
Crystallographic data and refinement statistics

	ΔN-ChoKα1·ADP·HC-3	ΔN-ChoKβ·ADP·Pho-HC-3
Protein Data Bank code	3G15	3FEG
Diffraction data		
Unit cell parameters (Å)	$a = 55.8$ $b = 119.0$ $c = 131.0$	$a = 98.0$ $b = 73.0$ $c = 62.4$ $\beta = 117.8°$
Space group	$P2_12_12_1$	$C2$
No. of molecules per asymmetric unit	2	1
Resolution range (Å)[a]	50–1.7 (1.76–1.70)	30–1.3 (1.35–1.30)
Unique reflections	93,657 (7,162)	92,472 (7,750)
Data completeness (%)	97.0 (75.6)	97.6 (82.4)
R_{sym} (%)[b]	6.9 (79.7)	4.0 (55.9)
Redundancy	6.5 (2.6)	3.6 (2.4)
Average $I/\sigma(I)$	31.6 (1.2)	36.3 (1.6)
Refinement statistics		
R_{work} (%)[c]/R_{free} (%)	22.0/25.7	15.8/19.3
No. of atoms		
Protein	5,388	2,872
Ligand/ion	128	124
Water	324	299
Root mean square deviation from ideal		
Bond length (Å)	0.015	0.017
Bond angles (°)	1.4	1.5
Average B-factors, Å^2		
Protein	27.2	17.7
Ligand/ion	30.1	21.8
Water	32.4	26.2
Ramachandran plot (%)		
Most favored	95.2	95.2
Additional allowed	4.6	4.5
Generously allowed	0.2	0.3
Disallowed	None	None

[a] Values in parentheses are for the highest resolution shell.
[b] $R_{sym} = \Sigma|(I - \langle I \rangle)|I?(I)$, where I is the observed intensity.
[c] $R_{work} = \Sigma||F_{obs}| - |F_{calc}||\Sigma|F_{obs}|$, where $|F_{obs}|$ and $|F_{calc}|$ are observed and calculated structure factor amplitudes, respectively.

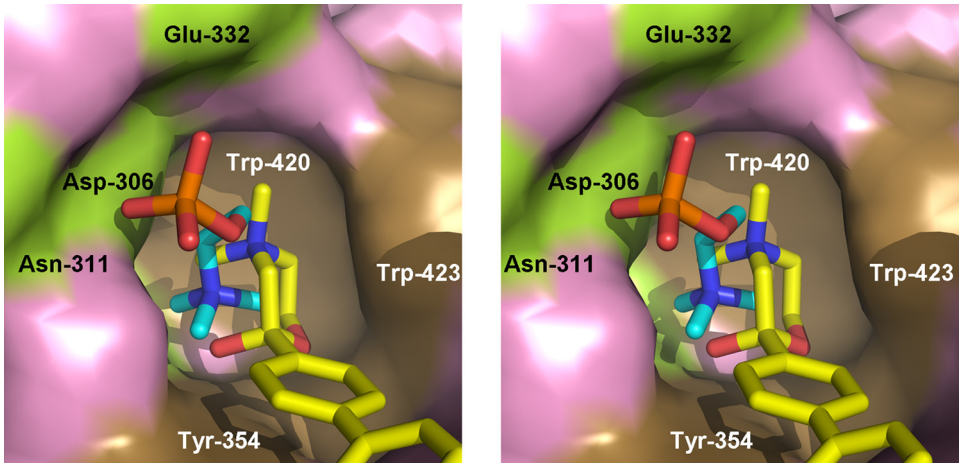

FIGURE 4. **Close-up *stereo view* of HC-3 and Pho-Cho superimposed on the choline-binding pocket.** The structure of the ChoKα·Pho-Cho complex (PDB code 2CKQ) overlaid on the crystal structure of the ΔN-ChoKα1·ADP·HC-3 complex (*pink surface*), and the ligands shown in the comparison reflect only the protein superposition. Both Pho-Cho and HC-3 are represented in *stick mode* and are colored *cyan* and *yellow*, respectively. Some of the key residues forming the choline-binding pocket are indicated, and the hydrophilic residues, including a catalytic base (Asp-306), and the hydrophobic residues are shown in *green* and *brown surfaces*, respectively.

nearly identical orientations of the conserved hydrophobic residues forming the binding groove (Fig. 6*A*). Of special interest, however, was the unexpected phosphorylation of HC-3 co-crystallized with ΔN-ChoKβ protein. As shown in Fig. 3*C* and supplemental Fig. S1*B*, the sigma-weighted $F_o - F_c$ omit map clearly showed tetrahedral electron density connected to the opened ring of HC-3 inside the choline-binding site. Atomic details of the interactions between Pho-HC-3 and surrounding residues are shown in Fig. 2*C*. Our ΔN-ChoKβ model also included further structural observations in supporting phosphorylation of HC-3. First, although the electron density corresponding to the adenosine moiety of the nucleotide was relatively clear, it was difficult to fit the phosphate groups owing to disordered or ambiguous electron density (supplemental Fig. S1*B*), suggesting the possibility that bound ADP was partly converted to AMP. Likewise, the second magnesium ion that coordinated the ADP β-phosphate in the ΔN-ChoKα1 model seemed to be released and replaced by a water molecule in the ΔN-ChoKβ structure (see supplemental Material II for details and supplemental Fig. S2*B*). Finally, the nucleotide-binding loop (residues 75–82) was highly disordered (supplemental Fig. S1*B*), likely due to the perturbation of the nucleotide phosphate groups (*i.e.* the conversion of ADP to AMP). Mass spectrometry analysis excluded the possibility that HC-3 or its stock solution used for co-crystallization was contaminated by chemically modified products. These findings suggest that ΔN-ChoKβ phosphorylated HC-3 in the

presence of ADP, resulting in the release of the second magnesium ion and disorder of the nucleotide-binding loop.

Assessment of HC-3 Phosphorylation Activity—Given the possibility that ΔN-ChoKβ is capable of phosphorylating HC-3, additional experiments were performed to verify whether our crystallographic observations can be supported by experimental data indicating that the two ΔN-ChoK isoforms have different catalytic capabilities. The *in vitro* activity of ChoK was tested in the presence of HC-3 using ADP as in the crystallization conditions. After incubation, the reaction components were separated with reversed-phase HPLC and analyzed by mass spectrometry. In a preliminary experiment using ΔN-ChoKβ, we observed that the molecular mass of the major peak of native HC-3 was increased by 80 Da, corresponding to the molecular mass of a phosphate group (Fig. 5*A*), strongly supporting the idea that HC-3 is phosphorylated by the enzyme. In contrast, HC-3 was not phosphorylated by ΔN-ChoKα1 in the same assay (data not shown). Additionally, separation and quantification of ATP, ADP, and AMP by HPLC were done to analyze products after enzymatic reaction and rule out other possibilities such as ATP contamination. When only ADP was incubated with ΔN-ChoKβ, and reaction products were analyzed using HPLC, no ATP product was detected even after 20 h of incubation (supplemental Fig. S3). This indicates that there is no detectable enzymatic activity converting two ADP molecules to ATP and AMP in a manner similar to the reaction catalyzed by adenylate kinases.

We next performed an HPLC-based radioactivity assay using the full-length wild-type ChoK proteins to monitor the transfer of ^{32}P from hot ATP or ADP to HC-3. All of the wild-type ChoK isoforms were purified, and their activity verified using choline as a substrate (Table 2). In the presence of [γ-^{32}P]ATP, wild-type ChoKβ was active and phosphorylated HC-3, whereas little or no activity was observed with wild-type ChoKα enzymes (Fig. 5*B*). In a parallel assay using [β-^{32}P]ADP instead of hot ATP, a similar trend in HC-3 phosphorylation was observed, although wild-type ChoKβ catalyzed the reaction in the presence of ADP less efficiently than ATP (data not shown).

To further confirm a phosphotransfer reaction, we co-crystallized ΔN-ChoKβ with HC-3 in the presence of ATP (for data collection and structure refinement statistics, see supplemental Tables S1 and S2). In this crystal, HC-3 existed in a phosphorylated form, although the electron density corresponding to the phosphate groups of the nucleotide was disordered like that of ADP co-crystallized with the beta isoform (supplemental Fig. S4). As a negative control experiment, we also crystallized ΔN-ChoKβ in the presence of HC-3 and AMP. However, no electron density was observed for the nucleotide, and only weak density for HC-3, which was not sufficient to fully confirm the state of the HC-3 molecule (data not shown).

Interaction of HC-3 with Wild-type ChoKs—To investigate the potency of HC-3 as an inhibitor, we determined its inhibition constants (K_i values) in the presence of choline as a substrate and dissociation constants (K_D values) for wild-type ChoK enzymes (Table 2). The inhibitory effect of HC-3 was ~500 times higher toward the ChoKα isoforms than ChoKβ isoform, indicating that HC-3 is a more potent and selective inhibitor for ChoKα isoforms over ChoKβ. These data also show that ChoKα1 and ChoKα2 have similar sensitivity to HC-3. A similar trend was observed with K_D values (Table 2).

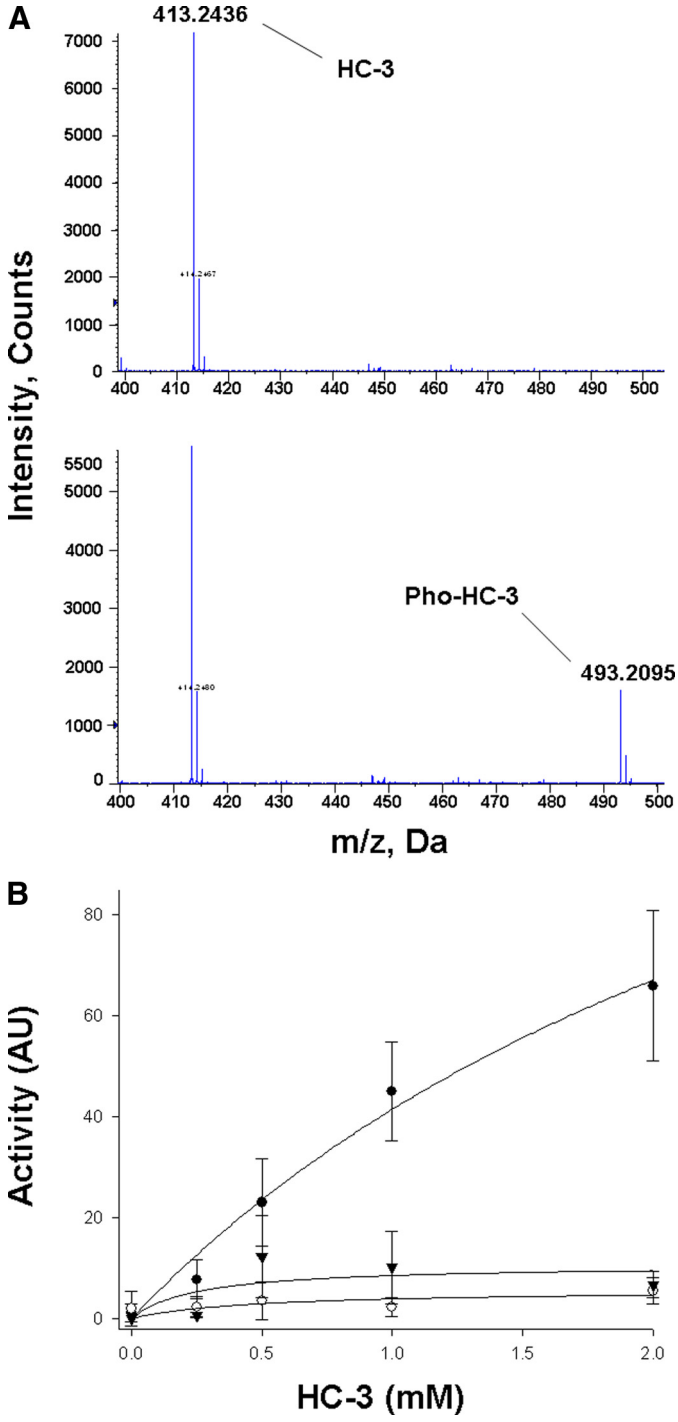

FIGURE 5. **HC-3 phosphorylation by ChoK.** *A*, mass spectra of the supernatant from a reaction mixture of ΔN-ChoKβ in the presence of ADP. The supernatant was incubated for 15 min and contains the major peak at *m/z* 413.2, corresponding to native HC-3 (*top*), whereas the spectrum from the same reaction mixture incubated for 5 h reveals the presence of another peak at *m/z* 493.2 corresponding to Pho-HC-3 (*bottom*). *B*, HC-3 phosphorylation activity by ChoK isoforms. The experiments were performed using full-length wild-type ChoKα1 (○), ChoKα2 (▼), and ChoKβ (·) in the presence of [γ-^{32}P]ATP. Data shown represent the means of triplicate determinations, and *error bars* indicate the standard deviations.

TABLE 2
In vitro characterization of wild-type ChoK isoforms and mutants

Protein	Choline			HC-3		
	K_m choline	K_m ATP	k_{cat}	Activity[a]	K_i[b]	K_D
	μM	μM	min^{-1}	%	μM	μM
ChoKα1-WT	180 ± 43	760 ± 140	4610 ± 380	<5	0.21 ± 0.01	0.10 ± 0.003
ChoKα2-WT	86 ± 44	400 ± 13	2840 ± 340	<5	0.23 ± 0.04	0.11 ± 0.007
ChoKα2-L401F	21 ± 7	400 ± 18	840 ± 130	83 ± 12	16 ± 3	0.84 ± 0.021
ChoKα2-L401A	107 ± 35	550 ± 160	2970 ± 505	ND	0.45 ± 0.07	0.12 ± 0.024
ChoKβ-WT	33 ± 14	400 ± 5	175 ± 60	100 ± 3	116 ± 15	45 ± 5
ChoKβ-F352L	41 ± 11	700 ± 16	275 ± 105	<5	5 ± 1.3	1.1 ± 0.1
ChoKβ-F352A	102 ± 41	650 ± 56	570 ± 265	<5	8 ± 1.5	1.5 ± 0.4

[a] Activity of each protein was determined using HC-3 and ATP as substrates.
[b] K_i value for the inhibitory effect of HC-3 on the activity of each enzyme was determined using choline and ATP as substrates.

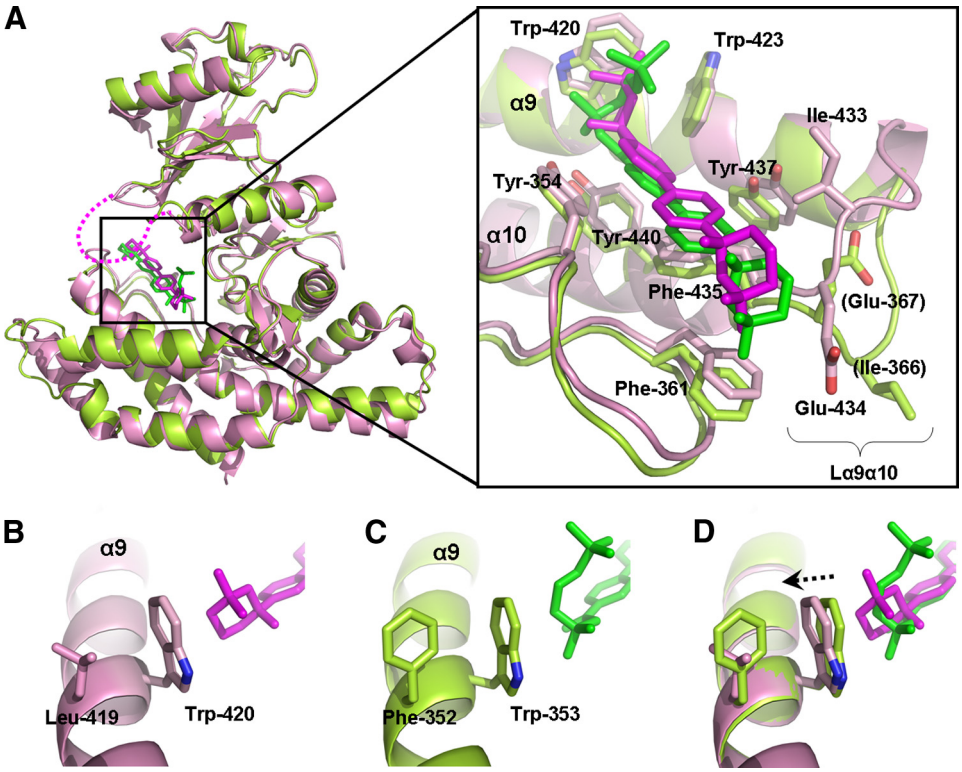

FIGURE 6. **Structural comparison around the HC-3-binding groove.** *A*, superposition of the crystal structures of both ΔN-ChoK ternary complexes. *Ribbon diagrams* for each structure are represented in the same colors as in Fig. 3. The disordered region, including 18 residues that are only present in ChoKα1, is schematically shown as a *pink dotted line*. HC-3 and Pho-HC-3 are colored *magenta* and *green*, respectively. The *inset* shows an *enlarged view* around the inhibitor-binding grooves of superimposed ternary complexes. The Lα9α10 region is indicated, and the residues that form hydrophobic contacts with HC-3 are shown in *stick representation* and labeled by the sequence number of ChoKα1. Two residues (Ile-366 and Glu-367) in ΔN-ChoKβ model that are excluded from the interaction with HC-3 due to a flipped-out conformation of Lα9α10 are indicated in *parenthesis* by the sequence number of ChoKβ. *B*, a *close-up view* of the interaction between Leu-419 and Trp-420 in the ΔN-ChoKα1·ADP·HC-3 complex structure. The side chains of these residues are arranged parallel to each other. *C*, a *close-up view* of the interaction between Phe-352 and Trp-353 in the ΔN-ChoKβ·ADP·Pho-HC-3 complex structure. These two side chains are oriented perpendicular to each other. *D*, a *close-up view* of superimposed *B* and *C*. The *dotted arrow* indicates the possible conformational change of the Trp-420 side chain upon HC-3 binding inside the choline-binding pocket of ΔN-ChoKα1.

Structural Differences between ChoK Isoforms upon HC-3 Binding—Due to the high sequence identity and structural similarity between ChoKα1 and ChoKβ, especially in the catalytic core and the HC-3-binding groove (Figs. 1 and 6*A*), the structural basis underlying differences in HC-3 phosphorylation and its inhibitory activity was not immediately obvious. However, detailed investigation of the subtle differences around the inhibitor-binding groove provided significant clues to address this question.

We have paid particular attention to the loop connecting helices α9 and α10 (Lα9α10). In the ΔN-ChoKα1 model, this loop was folded close to bound HC-3 (a "flipped-in" conformation), whereas the corresponding loop of ΔN-ChoKβ was positioned away from Pho-HC-3 (a "flipped-out" conformation) (Fig. 6*A*, *inset*). A comparison with previous ChoK structures suggests that the flipped-in loop in ΔN-ChoKα1 is conformationally conserved (supplemental Fig. S5*A*), whereas the flipped-out loop in ΔN-ChoKβ is likely an HC-3-dependent change (supplemental Fig. S5*B*). These conformational differences in Lα9α10 consequently affected the overall contact of the protein with the inhibitor molecule. Of the residues residing in Lα9α10 of ΔN-ChoKα1, Ile-433 formed a van der Waals interaction with the biphenyl moiety of HC-3, and the hydrocarbon segment of Glu-434 supported the solvent-exposed oxazinium ring of HC-3 (Fig. 6*A*). These two residues contributed to the formation of a restrictive and tight hydrophobic groove for HC-3. On the other hand, no direct contact was observed between the corresponding residues of ΔN-ChoKβ (Ile-366 and Glu-367) and the inhibitor (Fig. 6*A*). Relatively high temperature factors and weak electron densities of the solvent-exposed oxazinium atoms also suggest limited contact with the flipped-out loop conformation (supplemental Table S3 and Fig. 3*C*).

A second difference between the ΔN-ChoK models was observed near the choline-binding pocket. In ΔN-ChoKα1, one face of the Trp-420 side chain interacted with the oxazinium ring of HC-3, whereas its other face contacted the side chain of Leu-419 (Fig. 6*B*). Interestingly, this leucine residue is replaced

by phenylalanine (Phe-352) in ChoKβ (Fig. 1), which was oriented perpendicular to the side chain of Trp-353 (corresponding to Trp-420 of ΔN-ChoKα1) in our model (Fig. 6*C*). Upon HC-3 binding, the Trp-420 side chain of ΔN-ChoKα1 appeared to be pushed backward, thus offering space to accommodate HC-3 (Fig. 6*D*) and maintaining the flipped-in conformation of Lα9α10. In ΔN-ChoKβ, however, the shift of the Trp-353 side chain seemed to be restrained because of the bulky aromatic side chain of Phe-352 (Fig. 6*D*). The limited flexibility of Trp-353 might cause the flipped-out conformation of Lα9α10 to provide extra space for HC-3, thereby removing or lessening a putative steric hindrance between the inhibitor molecule and the binding groove. Taken together, these structural observations raised the possibility that the high HC-3 sensitivity of ChoKα1 compared with that of ChoKβ may be due to the different flexibility between the binding grooves of the two isoforms.

Characterization of ChoK Mutants—Based on the aforementioned experimental data and structural analyses, we hypothesized that Leu-419 of ChoKα1, or the corresponding Phe-352 residue of ChoKβ, could play an important role in regulating the interaction between HC-3 and the binding groove on the C-terminal lobe, and that the low binding affinity of HC-3 is related to its phosphorylation status. To test these ideas, a panel of single-amino acid-substituted mutants was constructed using full-length wild-type ChoK isoforms as templates. It should be noted here that the ChoKα2 isoform was mutated instead of ChoKα1 for several considerations. First, the alternatively spliced isoform ChoKα2 lacks an 18-residue segment (155–172 in ChoKα1, see Fig. 1) that is also missing in ChoKβ, making ChoKα2 a more comparable complement. Although disordered in our model and in that described by others (9), this segment was predicted to reside in the vicinity of the HC-3-binding groove (Fig. 6*A*) and, therefore, may have complicated any comparisons with ChoKβ. Likewise, ChoKα1 and ChoKα2 share similar enzymatic phenotypes toward HC-3 phosphorylation and inhibitory activity, which are clearly distinct from those of ChoKβ. The first mutant set included mutants in which Leu-401 of ChoKα2 (equivalent to Leu-419 of ChoKα1) was changed to phenylalanine (named ChoKα2-L401F), and the corresponding residue in ChoKβ, Phe-352, was changed to leucine (named ChoKβ-F352L). A second set was constructed by substituting these two residues with alanine to induce an artificial conformational flexibility of the conserved tryptophan residue upon HC-3 binding (named ChoKα2-L401A and ChoKβ-F352A).

As summarized in Table 2, ChoKα2-L401F showed ~70- and 8-fold increases in K_i and K_D values, respectively, as compared with wild-type ChoKα2, whereas the K_i and K_D values of ChoKα2-L401A were similar to wild-type ChoKα2. In contrast, both ChoKβ-F352L and ChoKβ-F352A exhibited significantly lower K_i and K_D values (~19- and 36-fold, respectively) compared with wild-type ChoKβ. These results indicate that the overall tendency of different ChoK isoforms to bind HC-3 could be affected by a single amino acid. Therefore, the leucine-phenylalanine variation between the ChoK isoforms is likely to be an important determinant in the inhibitory effects of HC-3.

Furthermore, ChoKα2-L401F gained the ability to phosphorylate HC-3 with an activity comparable to that of wild-type ChoKβ (83 and 100% for ChoKα2-L401F and ChoKβ-WT, respectively), whereas ChoKβ-F352L showed complete loss of the ability to phosphorylate HC-3 as compared with wild-type (<5 and 100% for ChoKβ-F352L and ChoKβ-WT, respectively). Both of the alanine-substituted ChoK mutants showed no or very low activity with HC-3 (Table 2). Measurements of ChoK activity using HC-3 as a substrate were rather qualitative due to the experimental conditions and very slow turnover for HC-3 phosphorylation. Consequently, the activity values with HC-3 are expressed as percentages in Table 2. All ChoK mutants were fully active in the presence of choline, suggesting that the mutation of Leu-401 in ChoKα2 or Phe-352 in ChoKβ had no significant effect on their overall ability to phosphorylate choline (Table 2). Taken together, these findings strongly support the idea that the interaction of HC-3 with the binding groove depends on the side-chain size of the amino acid residue neighboring the choline-binding site, which in turn affects phosphorylation of HC-3. A possible mechanism of HC-3 phosphorylation by ChoKβ will be discussed in detail below.

DISCUSSION

The ability of HC-3 to inhibit the activity of the ChoKα isoforms is in sharp contrast to its ability to be phosphorylated by ChoKβ. From our structural analyses, it initially appeared that flexibility of the conserved tryptophan residue (*i.e.* Trp-420 of ChoKα1 and Trp-353 of ChoKβ) that participated in the formation of the HC-3-binding groove may play a role in accommodating the inhibitor. Residue Leu-401 of ChoKα2, corresponding to Leu-419 of ChoKα1, or Phe-352 of ChoKβ, was identified as being important for conveying either inhibition by, or phosphorylation of, HC-3. This finding is particularly intriguing, given that Leu-419 in ChoKα1, or Phe-352 in ChoKβ, was not directly involved in the formation of the HC-3-binding groove. According to our assay results, exchange of these leucine and phenylalanine residues was sufficient to swap their HC-3 phenotypes in a reciprocal fashion, without loss of the typical ChoK enzyme function. Furthermore, when compared with wild type, ChoKβ-F352A had significantly enhanced affinity for HC-3, supporting the idea that the available space, created by residues with relatively small side chains (*i.e.* leucine and alanine), behind the conserved tryptophan residue is significant for the accommodation of HC-3. Conversely, a narrow space, created by phenylalanine with a bulky side chain, at the same position limited the conformation of the conserved tryptophan. This results in decreased structural elasticity of the HC-3-binding groove. This is also reflected in the low or reduced affinity binding of HC-3 to wild-type ChoKβ and ChoKα2-L401F (Table 2). Initially, the IC_{50} values of HC-3 were measured for the ChoK isoforms in the presence of choline as a substrate, which also supported that the ChoKα isoforms are more sensitive (at least 85-fold) to HC-3 than the β isoform (data not shown). However, our crystal structures indicated that the HC-3-binding site of each ChoK isoform overlaps with that of choline, which raised the possibility that the differences in IC_{50} values for the inhibitor might be due to differences between the K_m values of each ChoK isoform for choline. To

clarify this point, more detailed kinetic studies were performed, and the results were consistent with our conclusion based on IC_{50} values. Furthermore, our ITC results clearly revealed that there is a significant difference between the affinities of ChoK isoforms for HC-3 in the absence of choline, which correlates well with the K_i values for HC-3 (Table 2). Meanwhile, a recent study reported K_m values for choline using extracts of *E. coli* expressing human ChoK enzymes (48), wherein the K_m value of ChoKα1 for choline was 0.2 mM, consistent with our results (180 ± 43 μM). However, the K_m for choline of ChoKβ (0.57 mM) was at least an order of magnitude higher than what we report here (33 ± 14 μM). This difference may be partly related to possible negative cooperativity and the range of substrate concentrations used for determining Michaelis constants (see "Experimental Procedures"). Different assay conditions and/or impurities present in cell crude extracts could also be other contributing factors.

A unique observation of this work is the correlation of HC-3 phosphorylation with a lack of structural elasticity of the binding groove in the ChoKβ isoform. This correlation was also confirmed by our mutational studies, in which the reduced sensitivity toward HC-3 was accompanied by HC-3 phosphorylation, whereas the conferral of HC-3 sensitivity abolishes phosphorylation (Table 2). Through intramolecular attack of a hydroxyl group, the oxazinium moiety of HC-3 is expected to exist in equilibrium as hemiketal (cyclic) and hydroxy ketone (open) forms (36, 37) (supplemental Fig. S6*A*), which was considered as a clue to understand the above phenomenon. In the ΔN-ChoKα1 model, the high affinity interaction of HC-3 with the binding groove restrained the conformation of the HC-3 oxazinium ring inside the choline-binding pocket, wherein its hydroxyl group was oriented away from Asp-306, which is proposed as the putative catalytic base (9, 38, 39) (Fig. 4 and supplemental Fig. S6*B*). On the other hand, the rearrangement of Lα9α10 in the ΔN-ChoKβ structure was predicted to weaken the interaction with the inhibitor molecule, thereby permitting the binding of different conformations of the HC-3 oxazinium ring within the binding groove. However, it remains possible that the open form of HC-3 may be preferential for interacting with the binding groove of the ChoKβ isoform, albeit with low affinity. In our ΔN-ChoKβ model, the hydroxyl group of the open form of HC-3 was shown to be activated by Asp-242, corresponding to Asp-306 of ChoKα1, for phosphorylation (supplemental Fig. S6*C*). Additional analysis based on the superimposed structures of ΔN-ChoKβ·ADP·Pho-HC-3 and ChoKα·Pho-Cho revealed that the phosphorylated moiety of Pho-HC-3 overlays well with the Pho-Cho molecule (supplemental Fig. S6*C*), suggesting that the phosphorylation of HC-3 and choline is mediated by the same conserved catalytic module. Phosphorylation of HC-3 by ChoKβ was slow, even in the presence of ATP, making it difficult to determine accurate kinetic parameters. The poor affinity of ChoKβ for HC-3 may be a reason for this weak activity. It is likely that extended preincubation of protein and HC-3 during co-crystallization has provided an excellent condition for HC-3 phosphorylation. In this study, we were not able to obtain a co-crystal of ChoKβ and HC-3 in the presence of AMP. This suggests that the phosphorylation of HC-3 is a critical factor for co-crystallization with the beta isoform.

The HC-3 molecule is composed of a central hydrophobic biphenyl ring and two cholinomimetic oxazinium rings. Each of the oxazinium rings includes a positively charged quaternary ammonium and a hydroxyl group. HC-3 has been used as a template for the design of new inhibitors, and the most potent inhibitors reported so far also contain 2-fold symmetrical, antiparallel structures like HC-3, and each possesses two quaternary ammonium rings connected by a hydrophobic spacer (20, 40). Quantitative structure-activity relationship analyses of HC-3 analogues have shown that the inhibitory potency of ChoK correlates well with both the charge on the ring nitrogen and the size of the central hydrophobic spacer (25–27, 40). These findings suggest that the inhibitor-binding site of ChoK is highly specific for predominantly hydrophobic molecules carrying positively charged nitrogens. According to our crystallographic data, one of the HC-3 oxazinium rings occupied a choline-binding pocket of negative electrostatic potential, whereas the biphenyl group, including the other oxazinium ring, tightly bound to the hydrophobic groove on the C-terminal lobe (supplemental Fig. S7). This could explain why the positively charged quaternary ammonium groups and the hydrophobic spacer in the potential ChoK inhibitors are essential for their potency. However, it is still questionable whether both oxazinium rings of HC-3 are necessary for binding, because the second oxazinium ring mainly contributed to the hydrophobic interaction with the binding groove as shown in our structure (Fig. 3*B*). For future inhibitor development, asymmetric molecules that comprise a single oxazinium ring and a hydrophobic anchor and cover the entire binding groove like HC-3 can be designed to test their binding or inhibitory potency.

The ChoK inhibitors that have been currently reported have more extended structures than that of HC-3, such that the inhibitor-binding groove defined in this study seems too short to accommodate such inhibitors. It is tempting to speculate that only half-molecules of such symmetrical, longer inhibitors interact with the binding groove. Interestingly, half-molecules of HC-3 derivatives are less potent than complete molecules (26), suggesting that both halves contribute cooperatively to the inhibitory activity of ChoK. Owing to the unsuitable distance or arrangement between the two hydrophobic grooves of the dimer, it is unlikely that long, symmetrical HC-3 derivatives bind to both binding grooves on a ChoK dimer. Instead, it is possible that another adjacent ChoK dimer in solution could interact with the second half-molecule of the inhibitor, or the third binding site on the monomer may interact with the other half-molecule as proposed recently (41, 42). Additional structural studies through co-crystallization with HC-3 derivatives will be essential for understanding their exact binding mechanism.

Acknowledgments—We thank Drs. Melanie A. Adams-Cioaba and Sirano Dhe-Paganon for valuable discussions and corrections.

REFERENCES

1. Pelech, S. L., and Vance, D. E. (1984) *Biochim. Biophys. Acta* **779,** 217–251
2. Kent, C. (1990) *Prog. Lipid Res.* **29,** 87–105
3. Aoyama, C., Liao, H., and Ishidate, K. (2004) *Prog. Lipid Res.* **43,** 266–281
4. Exton, J. H. (1990) *J. Biol. Chem.* **265,** 1–4
5. Aoyama, C., Nakashima, K., and Ishidate, K. (1998) *Biochim. Biophys. Acta* **1393,** 179–185
6. Aoyama, C., Nakashima, K., Matsui, M., and Ishidate, K. (1998) *Biochim. Biophys. Acta* **1390,** 1–7
7. Aoyama, C., Ohtani, A., and Ishidate, K. (2002) *Biochem. J.* **363,** 777–784
8. Peisach, D., Gee, P., Kent, C., and Xu, Z. H. (2003) *Structure* **11,** 703–713
9. Malito, E., Sekulic, N., Too, W. C., Konrad, M., and Lavie, A. (2006) *J. Mol. Biol.* **364,** 136–151
10. Katz-Brull, R., and Degani, H. (1996) *Anticancer Res.* **16,** 1375–1380
11. Nakagami, K., Uchida, T., Ohwada, S., Koibuchi, Y., Suda, Y., Sekine, T., and Morishita, Y. (1999) *Jap. J. Cancer Res.* **90,** 419–424
12. Nakagami, K., Uchida, T., Ohwada, S., Koibuchi, Y., and Morishita, Y. (1999) *Jap. J. Cancer Res.* **90,** 1212–1217
13. Ramírez de Molina, A., Rodríguez-González, A., Gutiérrez, R., Martínez-Piñeiro, L., Sánchez, J., Bonilla, F., Rosell, R., and Lacal, J. C. (2002) *Biochem. Biophys. Res. Commun.* **296,** 580–583
14. Iorio, E., Mezzanzanica, D., Alberti, P., Spadaro, F., Ramoni, C., D'Ascenzo, S., Millimaggi, D., Pavan, A., Dolo, V., Canevari, S., and Podo, F. (2005) *Cancer Res.* **65,** 9369–9376
15. Lacal, J. C., Moscat, J., and Aaronson, S. A. (1987) *Nature* **330,** 269–272
16. Macara, I. G. (1989) *Mol. Cell Biol.* **9,** 325–328
17. Ratnam, S., and Kent, C. (1995) *Arch. Biochem. Biophys.* **323,** 313–322
18. Jiménez, B., del Peso, L., Montaner, S., Esteve, P., and Lacal, J. C. (1995) *J. Cell Biochem.* **57,** 141–149
19. Cuadrado, A., Carnero, A., Dolfi, F., Jiménez, B., and Lacal, J. C. (1993) *Oncogene* **8,** 2959–2968
20. Hernández-Alcoceba, R., Saniger, L., Campos, J., Núñez, M. C., Khaless, F., Gallo, M. A., Espinosa, A., and Lacal, J. C. (1997) *Oncogene* **15,** 2289–2301
21. Lacal, J. C. (1999) *Eur. J. Cancer* **35,** S133
22. Ramírez de Molina, A., Sarmentero-Estrada, J., Belda-Iniesta, C., Tarón, M., Ramírez de Molina, V., Cejas, P., Skrzypski, M., Gallego-Ortega, D., de Castro, J., Casado, E., García-Cabezas, M. A., Sánchez, J. J., Nistal, M., Rosell, R., González-Barón, M., and Lacal, J. C. (2007) *Lancet Oncol.* **8,** 889–897
23. Ramírez de Molina, A., Gallego-Ortega, D., Sarmentero-Estrada, J., Lagares, D., Gómez Del Pulgar, T., Bandrés, E., García-Foncillas, J., and Lacal, J. C. (2008) *Int. J. Biochem. Cell Biol.* **40,** 1753–1763
24. Glunde, K., and Bhujwalla, Z. M. (2007) *Lancet Oncol.* **8,** 855–857
25. Campos, J., Núñez, M. D., Rodríguez, V., Gallo, M. A., and Espinosa, A. (2000) *Bioorg. Med. Chem. Lett.* **10,** 767–770
26. Conejo-García, A., Campos, J., Sánchez, R. M., Rodríguez-González, A., Lacal, J. C., Gallo, M. A., and Espinosa, A. (2003) *Eur. J. Med. Chem.* **38,** 109–116
27. Conejo-García, A., Entrena, A., Campos, J. M., Sánchez-Martin, R. M., Gallo, M. A., and Espinosa, A. (2005) *Eur. J. Med. Chem.* **40,** 315–319
28. Hamza, M., Lloveras, J., Ribbes, G., Soula, G., and Douste-Blazy, L. (1983) *Biochem. Pharmacol.* **32,** 1893–1897
29. Otwinowski, Z., and Minor, W. (1997) *Methods Enzymol.* **276,** 307–326
30. Read, R. J. (2001) *Acta Crystallogr. Sect. D Biol. Crystallogr.* **57,** 1373–1382
31. Emsley, P., and Cowtan, K. (2004) *Acta Crystallogr. Sect. D Biol. Crystallogr.* **60,** 2126–2132
32. Murshudov, G. N., Vagin, A. A., and Dodson, E. J. (1997) *Acta Crystallogr. Sect. D Biol. Crystallogr.* **53,** 240–255
33. Davis, I. W., Leaver-Fay, A., Chen, V. B., Block, J. N., Kapral, G. J., Wang, X., Murray, L. W., Arendall, W. B., 3rd, Snoeyink, J., Richardson, J. S., and Richardson, D. C. (2007) *Nucleic Acids Res.* **35,** W375–W383
34. Kabsch, W., and Holmes, K. C. (1995) *FASEB J.* **9,** 167–174
35. Scheeff, E. D., and Bourne, P. E. (2005) *PLoS Comp. Biol.* **1,** 359–381
36. Sheff, K. Y., Yorek, M. A., and Long, J. P. (1990) *J. Pharmacol. Exp. Ther.* **255,** 357–363
37. Albert, B. J., Sivaramakrishnan, A., Naka, T., Czaicki, N. L., and Koide, K. (2007) *J. Am. Chem. Soc.* **129,** 2648–2659
38. Hon, W. C., Mckay, G. A., Thompson, P. R., Sweet, R. M., Yang, D. S., Wright, G. D., and Berghuis, A. M. (1997) *Cell* **89,** 887–895
39. Madhusudan Trafny, E. A., Xuong, N. H., Adams, J. A., Ten Eyck, L. F., Taylor, S. S., and Sowadski, J. M. (1994) *Protein Sci.* **3,** 176–187
40. Conejo-Garcia, A., Báñez-Coronel, M., Sánchez-Martín, R. M., Rodríguez-González, A., Ramos, A., Ramírez de Molina, A., Espinosa, A., Gallo, M. A., Campos, J. M., and Lacal, J. C. (2004) *J. Med. Chem.* **47,** 5433–5440
41. Milanese, L., Espinosa, A., Campos, J. M., Gallo, M. A., and Entrena, A. (2006) *Chemmedchem*. **1,** 1216–1228
42. Srivani, P., and Sastry, G. N. (2009) *J. Mol. Graph. Model.* **27,** 676–688
43. Thompson, J. D., Higgins, D. G., and Gibson, T. J. (1994) *Nucleic Acids Res.* **22,** 4673–4680
44. Gouet, P., Courcelle, E., Stuart, D. I., and Métoz, F. (1999) *Bioinformatics* **15,** 305–308
45. Allali-Hassani, A., Campbell, T. L., Ho, A., Schertzer, J. W., and Brown, E. D. (2004) *Biochem. J.* **384,** 577–584
46. Brostrom, M. A., and Browning, E. T. (1973) *J. Biol. Chem.* **248,** 2364–2371
47. Wallace, A. C., Laskowski, R. A., and Thornton, J. M. (1995) *Protein Eng.* **8,** 127–134
48. Gallego-Ortega, D., Ramirez de Molina, A., Ramos, M. A., Valdes-Mora, F., Barderas, M. G., Sarmentero-Estrada, J., and Lacal, J. C. (2009) *PLoS ONE* **4,** e7819